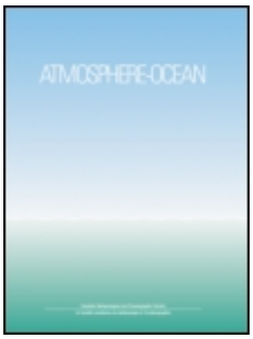

Atmosphere-Ocean

ISSN: 0705-5900 (Print) 1480-9214 (Online) Journal homepage: https://www.tandfonline.com/loi/tato20

The delineation of rain areas from visible and IR satellite data for GATE and mid-latitudes

S. Lovejoy & G.L. Austin

To cite this article: S. Lovejoy & G.L. Austin (1979) The delineation of rain areas from visible and IR satellite data for GATE and mid-latitudes, Atmosphere-Ocean, 17:1, 77-92, DOI: 10.1080/07055900.1979.9649053

To link to this article: https://doi.org/10.1080/07055900.1979.9649053

The Delineation of Rain Areas from Visible and IR Satellite Data for GATE and Mid-Latitudes

S. Lovejoy and G.L. Austin
Physics Department, McGill University, Montreal, P.Q.

[Original manuscript received 20 July 1978; in revised form 21 November 1978]

ABSTRACT *Two-dimensional pattern matching has been used to delineate raining areas of clouds from GATE and Montreal GOES visible and IR satellite data, with radar as ground truth. For the cases examined, the cloud cover was of the order of 4 times larger than the rain area, requiring skill to separate out low-thick or high-thin non-precipitating clouds from cumulus systems, which is difficult using a single threshold. The more flexible approach described here has allowed useful rain maps to be generated for all the types of weather systems examined. The optimum boundary separating raining from non-raining areas is relatively insensitive to diurnal and day-to-day variations, but is different for the tropical Atlantic and for Montreal.*

RÉSUMÉ *Une technique d'identification des configurations en deux dimensions a été utilisée pour déterminer à partir des données de ETGA et celles des ondes visibles et infra-rouges du satellite GOES reçues à Montréal, les endroits où il y avait des précipitations; les données de radar sont prises comme données réelles. Pour les cas examinés, la région couverte de nuages était environ 4 fois plus grande que la région de pluie, ce qui a necessitait la séparation des régions nuageuses où il n'y avait pas de précipitation en zones de nuages bas et epais et en zones de nuages hauts et minces, tâche qui aurait été difficile avec un seuil unique. L'approche plus flexible décrite ici nous a permis de produire des cartes des régions de pluie pour tous les systèmes météorologiques examinés. Le contour limite optimum séparant les régions pluvieuses des régions non pluvieuses est insensible aux variations diurnes et aux variations d'un jour à l'autre. Il est cependant différent pour l'Atlantique tropique que pour Montréal.*

1 Introduction

In quantitatively analyzing satellite data most researchers have concentrated on the important problem of the estimation of rain amounts. This project on the other hand has concentrated on using satellite data to delineate rain areas. These latter data are required as input into an objective real-time short-range forecast system called SHARP (Austin and Bellon, 1974; Bellon and Austin, 1978).

ATMOSPHERE-OCEAN 17 (1) 1979, 77–92 0705-5900/79/0000-0077$01.25/0

The problem reduces to determining the raining areas of clouds. Early studies have used people to classify the clouds subjectively (Follansbee, 1973; Barrett, 1970; Scofield and Oliver, 1977a, b; Ingraham et al., 1977) and then the amount of rain was estimated from the amount of time that an area was covered by rain-producing clouds. This method has been refined by using climatological rain rates (Follansbee and Oliver, 1975; Follansbee, 1976). These techniques have been used mostly for estimating rainfall over periods ranging from weeks to months. Other techniques have been developed for estimating rain amounts by following the expansion of anvils (Sikdar, 1972; Stout et al., 1977), and life histories (Griffith et al., 1978).

There have been other attempts at relating satellite brightness measurements to rainfall rates (Cheng and Rodenhuis, 1977; Blackmer, 1975; Silva Dias et al., 1977; Kilonsky and Ramage, 1976; Lovejoy, 1978). However, the visible and infrared (IR) wavelengths predominantly respond to the relative abundance of very small cloud particles and not to the precipitation sized particles. This is probably the reason why these studies have had little success in defining rain rates. Microwave sensors do respond to hydrometeors but have poor resolution ($\sim$50 km) and problems with surface emission, particularly over land, (Wilheit et al., 1977). We have felt, however, that the area of rain is of some interest in itself even if these schemes for estimating rain amount prove difficult in practical application. In particular, the use of the rain area in an overlay with synoptic charts or for short-range forecasts may be of considerable operational value.

2 Description of data used for the test

The satellite data were archived from the GOES system at Wisconsin. The radar data were obtained from the McGill Weather Radar located just outside Montreal, Canada and from a radar operated by McGill on CCGS *Quadra*, the Canadian ship which took part in the GATE experiment in 1974 in the tropical Atlantic.

The 46 satellite and radar data sets were analysed into common areas of 180-km range from the radar and into bins with 4 × 4 km spatial resolution.

3 Theoretical statement of the problem

To improve on previous attempts at rain area determination using visible or IR cutoffs (Stout et al., 1977; Griffith et al., 1978), the techniques of statistical pattern recognition have been used.

Statistical pattern recognition starts with the problem of resolving objects belonging to m different classes in n-dimensional space. Since the objects are statistically distributed, boundaries between classes are optimized to minimize some general loss function $f(x_1 \ldots x_m)$ where the $x_1 \ldots x_m$ are n-dimensional vectors representing the data distribution of the classes 1 to m. The minimization approach followed below, corresponds to Bayes decision theory.

For rainfall where we have to start with 2 classes – rain or no-rain (later

extended to 3 – no-rain, light rain, heavy rain) and have two variables – IR and visible brightnesses – therefore $n = m = 2$. In the following we assume the radar is an accurate ground truth with the implicit assumption that anything below the radar sensitivity of 0.5 mm hr^{-1} is not rain and anything above is rain. We thus define the following variables:

N_N = correctly classified no-rain
N_R = incorrectly classified no-rain
R_R = correctly classified rain
R_N = incorrectly classified rain.

Thus we may define our general loss function as:

$$f = (L_R R_N + L_N N_R)/(R + N) \qquad [R = R_R + R_N, N = N_R + N_N]$$

where L_R and L_N are losses arising from incorrectly classifying a point as rain and no-rain, respectively.

The obvious choice is to weight the penalty for R_N and N_R equally, i.e. $L_R = L_N = 1$. This reduces our problem to one of minimizing the fraction of false classifications $f = (R_N + N_R)/(R + N)$. Although ultimately this function was used, it is not transparently the best. As will be seen, often the loss function for $L_R = L_N = 1$ is almost minimized by saying that no rain falls anywhere, since the non-raining area is generally much greater than the raining area. This classification would have a loss function of: $f = R_N/(R + N)$ with $R_N = R =$ number of rain points, since obviously every case where it was raining would be incorrectly classified. If our more sophisticated scheme, which classified most of the rain and most of the no-rain correctly, produced errors of the order of R, then clearly our loss functions would have no well-defined minimum.

The obvious solution seemed to be to assign loss functions inversely proportional to the *a priori* probabilities; thus, putting $L_R = (N + R)/R$ and $L_N = (N + R)/N$, we obtain:

$$f_i = \frac{R_N}{R_N + R_R} + \frac{N_R}{N_N + N_R}.$$

A third statistic was also computed – the correlation coefficient (ρ) for the satellite generated rain map (based on one of the above optimization schemes), and the radar rain map. For the correlation coefficient rain is assigned the digit 1 and no-rain, 0. Thus, after suitable mathematics:

$$\rho = \frac{R_R N_N - R_N N_R}{RN}.$$

The problem with ρ and f_i is that they have no ready physical interpretation, whereas the original f is simply the fraction of errors. Putting heavy emphasis on getting the rain right at the expense of the no-rain we would choose to optimize f_i, since for a 5% coverage it would weight an incorrectly classified rain point 19 times more heavily than an incorrectly classified no-rain point. To get the approximately correct position and area of the rain, however, f is chosen as an equitable weighting scheme.

4 Scoring schemes

These optimized loss functions will be used to give rain area maps. A major problem connected with the satellite rain maps is that of determining their accuracy for various applications. For an observer at a single point on the ground who seeks a satellite estimate at a given instant, the statistic of importance is clearly the percentage of the satellite map that is correct. However, if we are interested in tracking satellite defined rain areas or in using them for estimating parameters as inputs to meso-scale forecasting programmes, then we need another measure of accuracy.

It was to this end that a special subprogram was developed to "score" the satellite map. The essential point was the recognition that when the satellite rain map and radar rain map disagreed, they tended nonetheless to predict rain in physically adjacent areas. Thus, to a certain extent, the effects of the two errors N_R and R_N are unimportant in an operational scheme if they occur in close physical proximity – on a scale smaller than that of interest.

A scale of 40 km was chosen (so as to give a statistically significant number of 4 × 4 km data points), and thus the 400 km × 400 km image was broken up into 100 boxes 40 km × 40 km. This resolution is comparable to the Tiros-N microwave data, and allows statistical description of the fractional rain coverage of a Tiros-N resolution cell. Since the microwave estimated rain amounts depend non-linearly on the fractional rain area coverage such a characterization is potentially useful. In each box the radar percentage coverage was compared with the satellite percentage coverage, and the difference recorded as the error at the 40 km × 40 km resolution. It was thus possible to make statements of the form "75% of the time, the satellite rain map is correct within $\pm X\%$ of the rain area with a resolution of 40 km". This is the so-called "75% confidence limit" of Table 1 (a, b). We feel that for many purposes, this is a more useful description of the accuracy than specifying the fraction of incorrect points.

5 Data analysis

The analysis outlined in Section 2 requires a 2-D frequency plot of the satellite data for the radar-determined rain and no-rain data points separately. The 4 × 4 km visible and IR data were scaled and accumulated in a 25 × 25 array as shown in Fig. 1a, b. The 25 levels rather than the raw data (64 for visible and 256 for IR) were chosen to give a relatively larger number of points in a sizable number of the 25 × 25 array elements. The normalization procedure represented an attempt to deal with the visible data sunlight normalization problem, and consisted of spreading out the data into 25 levels between its maximum and minimum values. The simplistic assumption was that the maximum visible brightness was essentially reflectance from an optically infinite thick cloud and that the rest of the reflectance values were linearly scaled. Specifically, the brightest and dimmest points in the visible field over the radar were chosen, and all the visible values were subsequently linearly transformed onto the interval [0, 1]. From each distribution, the visible and IR mean, standard deviation and correlation were computed.

TABLE 1. Characteristics and error statistics of GATE and Montreal data

Day	Time	Cloud Cover %	Rain Coverage %	Error ($f \times 100$) %	75% Confidence Limit %	Inverse Loss Functions (f_l)	$P_{RN} \times 100$	$P_{LH} \times 100$	Corr. Coeff. (ρ)
a) GATE Data									
251	1300	59.3	10.4	9.5	8	0.509	6.0	61.8	0.489
252	1300	75.1	30.5	17.7	11	0.409	30.1	68.3	0.590
247	1300	59.5	15.4	10.2	7	0.328	0.07	51.4	0.671
242	1300	39.4	5.1	4.2	5	0.448	6.5	99.8	0.552
246	1300	62.7	6.5	5.7	8	0.774	81.0	99.0	0.225
243	1300	14.5	2.5	1.9	1	0.735	66.1	88.7	0.264
248	1300	85.0	45.1	15.2	15	0.306	4.4	37.0	0.694
261	1300	11.5	8.2	10.1	10	0.630	77.0	75.8	0.370
b) Montreal Data									
180	1500	94.8	24.5	15.4	10	0.413	30.6	84.3	0.587
180	1530	91.8	23.7	18.9	15	0.579	23.4	90.0	0.421
180	1600	89.9	24.1	19.6	15	0.621	30.5	92.7	0.397
180	1630	88.0	24.9	18.4	15	0.583	21.5	80.2	0.417
180	1700	83.7	23.5	16.4	14	0.589	10.9	82.9	0.410
180	1730	81.5	23.4	14.7	15	0.400	6.7	83.9	0.600
153	1730	73.3	13.7	10.9	10	0.432	5.3	91.7	0.567
153	1800	74.1	16.5	13.6	10	0.477	13.4	98.5	0.522
153	1830	74.5	16.5	14.0	10	0.433	16.8	99.5	0.567
153	1900	77.4	17.0	14.2	12	0.491	22.4	99.9	0.508
152	1730	84.7	11.9	6.2	5	0.26	1.1	95.8	0.739
152	1800	84.9	10.9	8.2	6	0.317	1.9	92.1	0.683
152	1830	82.9	9.9	8.6	6	0.384	14.2	92.5	0.616
152	1900	83.6	7.8	8.3	10	0.547	2.6	71.7	0.453
152	1930	86.4	9.1	9.0	10	0.471	39.0	60.1	0.529
152	2000	85.3	9.5	10.8	10	0.590	40.0	90.6	0.410
152	2030	82.1	8.8	14.6	15	0.578	53.4	82.6	0.423

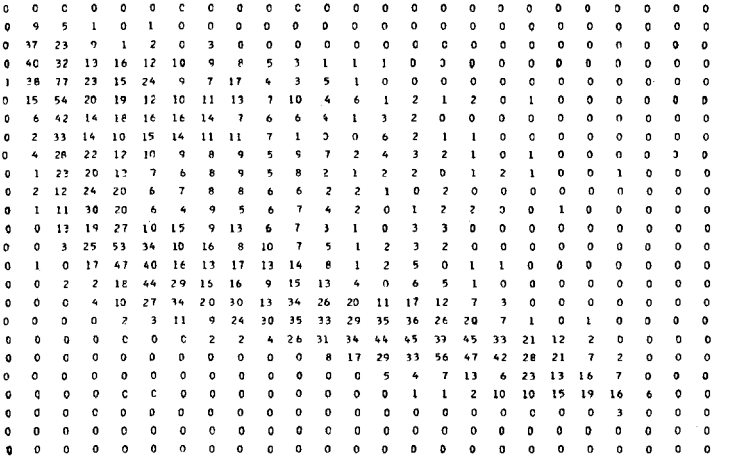

Fig. 1a

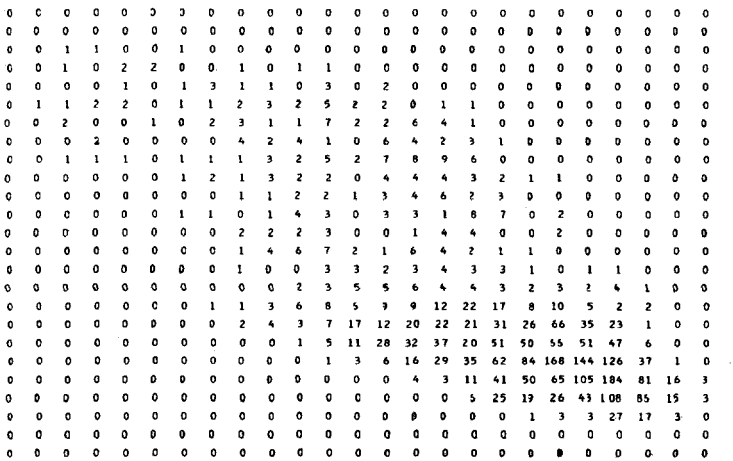

Fig. 1b

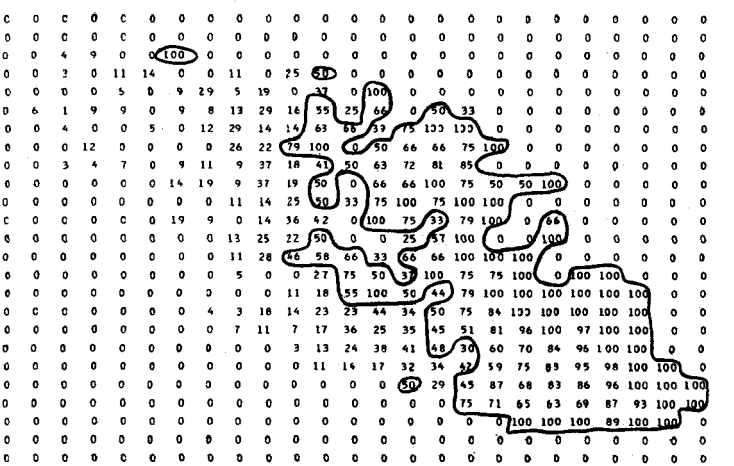

Fig. 1c

6 Results

For all cumulus situations in GATE or Montreal, the rain data were scattered about the high visible, high IR (cold) end of the diagram as expected (Fig. 1b). This distribution was to a good approximation a two-dimensional Gaussian. The no-rain distribution however was quite different – it was often bimodal (Fig. 1a), with one peak centred at low visible low IR values and the other near the rain peak, but always at least slightly shifted in the low visible, low IR direction. Clearly, these were data from clouds associated with the rain clouds, but which were not raining. This interpretation was borne out by an examination of the photographic images which demonstrated their physical proximity. Table 1a, b shows that in general the cloud cover (IR colder than 5°C) was ~80% for Montreal and ~40% for GATE for the data sets used in this analysis. The rain areas were smaller by a factor ~4 showing that significantly greater skill is required to define the rain areas.

a *Statistical Tests*

If the rain and no-rain samples were approximately Gaussian, one could apply a two-dimensional version of the traditional χ^2 test to determine the probability that the two samples came from the same population. A small probability would indicate that a classification scheme based on satellite data would be physically meaningful, since the probability would be high that we really were dealing with two different populations rather than 2 different samples of the same population.

Using the conventional maximum likelihood method the most likely mean and standard deviation (in a co-ordinate system with independent random variables) were determined, and also the probability of the rain and no-rain samples coming from the same population (denoted P_{RN}). In most cases of cumulus activity the probability was low – almost always less than 50% and often less than 10% (Tables 1a, b: 8th column). This must be regarded as an over-estimate since the no-rain distribution is clearly not Gaussian and thus the effective Gaussian mean was shifted more towards the no-rain mean, than would otherwise have been the case.

In any event this test was not considered important for the rain/no-rain plots but as will be seen below was used extensively in the light rain/heavy rain classifications, where both distributions were close approximations to Gaussian shape.

Fig. 1a Frequency plot of no-rain distribution for GATE day 248, 1300 GMT. Horizontal axis is visible data on scale 0–1, and vertical axis temperature also normalized on scale 0–1.

Fig. 1b Similar to 1a, for rain data.

Fig. 1c Elements of Fig. 1b as a percentage of Fig. 1a plus Fig. 1b, with the resulting optimum boundary sketched in. Any combination of visible and IR values within this boundary resulted in a satellite rain point. Anything outside resulted in a no-rain point. The resulting map is shown in Fig. 2.

b *Rainfall Rate Determination*

As mentioned earlier, the classification scheme mentioned was extended to the case of light rain and heavy rain in an effort to determine the extent to which rainfall rate information was contained in the satellite data. The definition of "heavy" rain, was arbitrary, but assigned a value of 2 mm h^{-1} (as determined by radar), chiefly because this seemed to give approximately equal amounts of heavy and light rain for most cumulus storms, and thus gave more reliable statistics. Higher rainfall rates yielded similar results.

The heavy rain plots were invariably shifted slightly towards the high IR high visible end of the diagram, as expected. The shift however, was so small that when the probability of them coming from the same population (denoted P_{LH}) was determined as described earlier, the probability was almost always at least 80% that the samples had come from the same population and often more than 90% (Table 1a, b: 9th column), although the slightly lower values in GATE suggest that some skill might be shown in separating heavily raining areas in the tropics.

It would thus appear that while rainfall/no-rainfall distinctions are well-founded, little if any rainfall-rate information is contained in a single satellite image.

c *Non-Cumulus Storms*

Non-cumulus storms were the usual storm type found after the end of August in the Montreal region. Only one good example was found, with over 20% coverage. The other examples contained typically 0.1 – 5% coverage, and thus had insufficient data to perform a good statistical analysis. While it should be stressed that the following conclusions are therefore based on a limited data base, compared with the cumulus results, they are none the less interesting.

The main feature of the no-rain plot was that it had lost its bimodal character and appeared as a broad 2-D Gaussian. The rainfall points seemed to lie entirely within this region, shifted slightly to the high visible end, but with about the same, if not lower IR mean. The probabilities of the two coming from the same population (P_{RN}) were typically greater than 50%, indicating the difficulty of even extracting rainfall area information from under low, thick clouds. Fig. 3 shows the rain map for the example discussed above.

7 Satellite rainfall map production using radar-assisted optimization

In order to get the classification scheme for the best rain area accuracy, we minimized the fraction of errors $f = (R_N + N_R)/(R + N)$. Because of the problem of local minima in this function particularly when near the no-rain anywhere classification we added the additional constraint, that the scheme classify approximately the same number of points into the rain category as there were radar-determined rain points, thus guaranteeing that the satellite-derived rain map had approximately the same area as the radar one.

The optimization procedure was thus straightforward – a 25 × 25 array

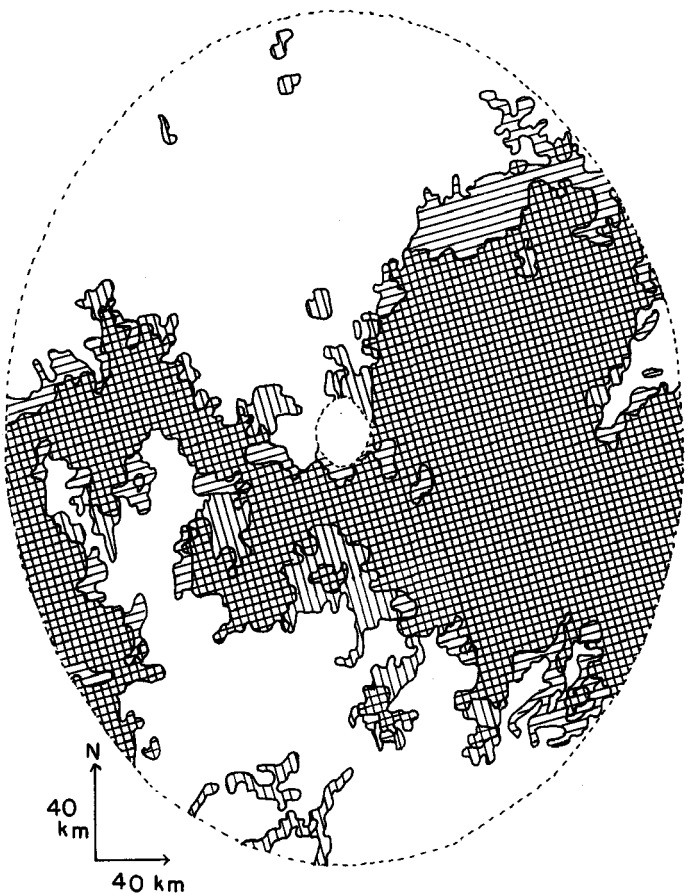

Fig. 2 The satellite rain map produced by the optimization of the data in Fig. 1. Vertical lines are radar rain areas, horizontal lines are satellite rain areas. The radar range is 180 km. Note that the percentage error (in this case = 15.2%) is not the percentage of the striped areas to cross-hatched areas, but is the percentage of the striped areas to areas cross-hatched or blank (the latter represented satellite and radar agreement on no-rain).

giving percentages of an IR-visible value that were covered by rain was calculated. The number of rain and no-rain points in 5% intervals was then determined, and finally, a sum of all points starting at 100% rain down to a value which approximately gave the correct number of rainfall points was determined – this was the critical percentage. A region of the IR-visible plane that contained points such that the percentage of rain out of the total points was greater than or equal to the critical percentage was included as a rain area.

A typical classification boundary as a result of the above analysis is shown in Fig. 1c with the resulting satellite rain map shown in Fig. 2. The small areas separated from the rest of the rain region contain very few points, i.e. 100% representing 1 rain point, 0, no-rain points. They may safely be attributed to the limitations of the small sample size. The same is true about the fine

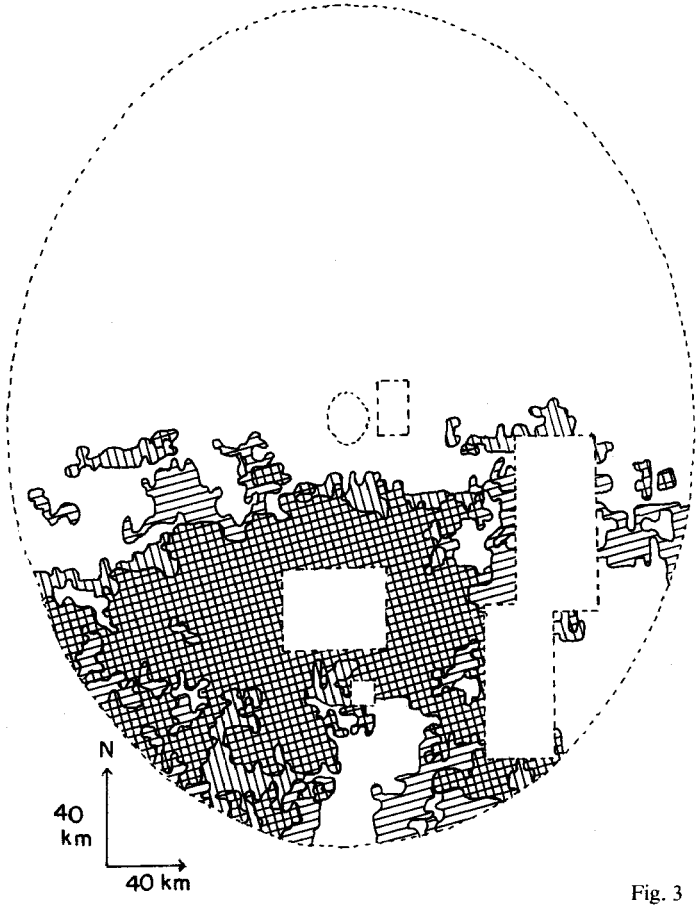

Fig. 3

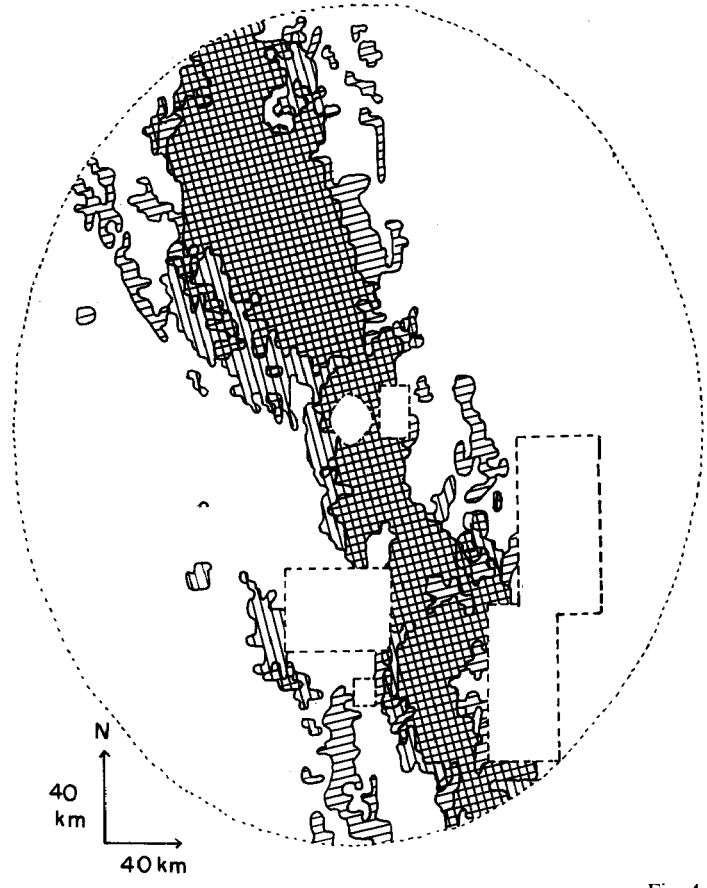

Fig. 4

structure of the boundary around the main area which varies greatly from image to image. What is encouraging is that the images all have rain boundaries at approximately the same position whether from GATE or Montreal and even at greatly varying times of the day, indicating the success of our visible normalization procedure. Examples of satellite rain maps produced for Montreal are shown in Figs. 3 and 4, for non-cumulus and cumulus cases, respectively.

8 Stability and accuracy analysis

The preceding results have all been based on the analysis of single images, and their optimization. Clearly however, if the technique is to be used operationally it is important to investigate the hour-to-hour, day-to-day and place-to-place stability of the optimum boundary.

The obvious way to do this is to accumulate statistics over a large number of images and make a "grand" optimization boundary. For comparing between different images it seemed clear that "normalizing" the spectral plots in the IR direction would reduce stability since temperature is a more fundamental parameter.

a *Montreal Data*

The next step that was taken, was to produce statistics for the three sequences of data available. The data used were all at $\frac{1}{2}$-h intervals within the sequence, consisting of 6 images (33738 pts) for day 180, 7 images (40361 pts) for day 152, and 4 images (22558 pts) for day 153. Optimum boundaries were determined for each of these days separately and compared. The relevant statistics are shown in Table 2. It is interesting to compare the optimum boundaries (Fig. 5). They all have remarkably similar shapes especially when one considers that the chief areas where differences are appreciable – the low visible "beak" on days 153 and 180 – contain relatively few data points. It should be noted that the cutoff of the optimum boundaries for high ($\gtrsim 0.85$) visible at IR temperatures less than 222 K appears to be a real feature of the Montreal data but not for GATE. It is possible that the difference is related to either the greater wind shear or lower tropopause in mid-latitudes.

To quantify the variability in estimates of satellite rain areas for the three sequences, the "grand" optimum boundary was applied to all of the images both individually and accumulated over the three sequences separately. Since there is no generally accepted statistic to represent the hour-to-hour or day-

---

Fig. 3 A satellite rain map of Montreal, day 256, 1977, showing that even with heavy stratus cover, and a 2-D frequency plot quite different from the cumulus cases shown in Fig. 5, that radar optimum boundary determination nonetheless gives a good map. In this case, the 75% confidence limit was 16% and the percentage coverage of rain was 23.7%. The areas blocked out are from mountains and other ground echo. The radar range is 180 km.

Fig. 4 A satellite rain map of Montreal, day 180, 1977, at 1630 GMT, showing an active cumulus band. The radar range is 180 km.

TABLE 2. Comparison of statistics which give an indication of map qualities

Day	Opt. 2-D Boundary	IR Optimum Threshold		Visible Optimum Threshold		Area Rain Coverage (%)	Total No. of Points
	$(R_R/R) \times 100$*	IR(K)	$(R_R/R) \times 100$	(Scale: 0–1)	$(R_R/R) \times 100$		
GATE							
242, 243, 246 247, 248, 251 252, 261	65	<232	53	>0.68	64	15.8	47706
Montreal							
152	56	<232	20	>0.88	31	9.7	40361
180	56	<247	55	>0.80	48	24.0	33738
153	53	<254	52	>0.88	49	15.9	22558

*Referred to in text as "percentage of correct satellite rain."

TABLE 3. Statistics indicating stability of various rain area estimation techniques. For a perfect technique: Bias = Error Factor = 1; $E_{RMS} = 0$

Technique	Region	Number of Images or Sequences	Bias	Error Factor	E_{RMS}
2-D Pattern Matching	Montreal	17	1.13	1.26	0.22
2-D Pattern Matching	Montreal	3	1.08	1.19	0.18
Optimum IR Threshold	Montreal	3	1.38	1.74	0.71
Optimum Visible Threshold	Montreal	3	1.54	1.59	0.58
2-D Pattern Matching	GATE	8	1.21	1.41	0.25

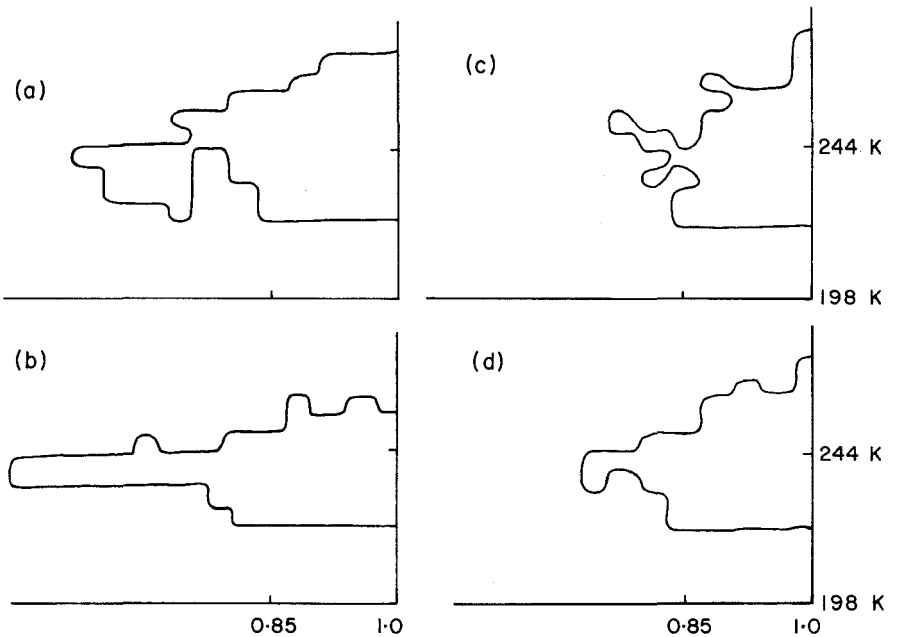

Fig. 5 An enlarged section of the two-dimensional optimum boundary similar to Fig. 1c, only with temperature scaled as indicated. The visible optimum threshold (= 0.85 on scale 0–1) is shown, as well as the IR optimum threshold (= 244 K) for Montreal (a) is day 153, (b) day 180, (c) day 152, and (d) is the ensemble optimum ("grand" optimum) boundary for all three.

to-day errors, we have included three statistics commonly used in the literature. The Bias (also known as "mean ratio") is defined as the average ratio of satellite determined area to radar determined area. The Error Factor is the mean of the ratio of the two areas such that the individual ratios are always greater than 1. E_{RMS} is defined as the root mean square difference of the two areas divided by the mean radar area. A perfect technique would yield a bias and error factor of 1 and an E_{RMS} of zero.

Since it is most sensitive to the accuracy of cases involving large areal coverage, we feel that of the three statistics, the latter gives the best idea of total areal accuracy.

Table 3 row 1 gives these three statistics for the 17 individual Montreal images, and row 2 indicates the same statistics when the individual images are accumulated into sequences. As expected, the errors decrease when we go from the individual image to sequence comparisons, since the data accumulation into sequences has a tendency to smooth out fluctuations from image-to-image. We feel that the technique demonstrates significant accuracy, especially when one considers that there were apparently substantial meteorological differences between the sequences, with day 152 for example containing both widespread cirrus and stratus components while the others were more convective in character.

b *GATE Data*

A similar analysis was carried out for the tropical Atlantic data. Unfortunately, we had no sequences and used 8 images on separate days. These also produced an optimum boundary. It is rather different in appearance than the Montreal boundaries, chiefly reflecting the lack of widespread low, thick cloud. The stability of this was investigated by a similar method to that of the Montreal data except here, only 8 images were available, with no sequences. The resulting error statistics are shown in Table 3 row 5.

Apparently, the scheme is less accurate for GATE than for Montreal, but the difference is not so large that statistical fluctuations caused by the small sample size could not have produced it.

However, as can be seen from Table 2, the optimum boundaries did better by about 20% in GATE than in Montreal relative to the percent of the satellite map which was correct. This was to be expected since the lack of low thick clouds and the colder convection tops all help separate raining from non-raining clouds. The apparent contradiction between less stability in GATE and more accurate maps arises from the fact that stability is determined by comparing the total predicted satellite areas with the radar areas, regardless of the physical proximity of the two maps.

9 Spectral thresholding

Most researchers when analyzing digital satellite data have used thresholds in the visible and IR domains to attempt to delineate rain areas. This is equivalent to restricting the spectral boundary discussed in this paper to lines parallel to the two axes. The existence of a meaningful threshold would have important implications, essentially because it would mean that only one of the spectral channels on the GOES satellites would have to be used to obtain a good rain area map. If the optimum channel happened to be IR then the limitations imposed by sun angle normalization, and day-time only availability would be removed.

The obvious method of avoiding the previous subjective method of threshold determination, was to use the same criterion of an optimum boundary, only confine the boundary to straight lines parallel to the axes of the 2-D frequency plot. For the sequences examined, the results are shown in Table 2.

What is interesting is that while for a given sequence the optimum IR or visible threshold is often almost as good as the optimum boundary, the optimum threshold does not show the same sequence-to-sequence stability that the optimum boundary does; on day 152 with widespread low and thick cloud as well as cirrus neither an optimum IR nor visible threshold is nearly as good as the optimum boundary (the visible threshold is 45% worse as measured by the percentage of correct satellite rain, and the IR threshold is 58% worse). In the other two sequences the IR, not the visible threshold, is better chiefly due to the exclusion of cold cirrus.

For an examination of the sequence-to-sequence error involved in using a single threshold for the three sequences we may construct rows 3 and 4 of Table 3 which compare the sequence-to-sequence error obtained by using the

best 2-D ("grand") (Table 3 row 1) boundary to the errors in the best IR and visible boundaries separately. Clearly the errors involved in using a "best threshold" are very large indeed. This should be expected, since the IR cannot remove cirrus components effectively and the visible cannot remove the low and thick cloud effectively. Both do a very poor job on the day where both are widespread (see row 2 Table 2).

Examining the GATE optimum thresholds (from Table 2), we find that visible thresholding does almost as good a job as the optimum boundary (only 1.5% worse) and that this is significantly (19.3%) better than the best IR threshold.

These results would seem to support and explain those of Stout et al. (1977), that visible images give less error in rainfall amount estimation than IR images. The fact that over GATE a visible threshold is almost as good as an optimum boundary could explain the relative success of the Sikdar (1972) scheme over GATE, but not over mid-latitudes.

10 Conclusions

Two-dimensional pattern matching has been used to delineate raining areas of clouds from GATE and Montreal GOES visible and IR satellite data, with radar as ground truth. For the cases examined, the cloud cover was of the order of 4 times larger than the rain area, requiring skill to separate out low-thick or high-thin non-precipitating clouds from cumulus systems, which is difficult using a single threshold. The more flexible approach described has allowed useful rain maps to be generated for all the types of weather systems examined here. The optimum boundary separating raining from non-raining areas is relatively insensitive to diurnal and day-to-day variations, but is different for the tropical Atlantic and Montreal. For widespread rain (stratus) days and convective days for Montreal, the optimum boundary is significantly different. In operational use, radar optimization in real-time over a small portion of the satellite image will be sufficient to produce a useful rain map.

Acknowledgements

We are deeply indebted to Dr Don Wylie at the University of Wisconsin who fulfilled the non-trivial task of procuring the GOES satellite data, and provided helpful criticism. Fruitful discussions were also held with Mr Fred Mosher and Dr Dave Martin. Mr Graham Morrissey of the Atmospheric Environment Service is also acknowledged for his support of the project. We would also like to thank Mr Aldo Bellon and Ms. Alamelu Kilambi of the Stormy Weather group for assistance with the data processing.

References

AUSTIN, G.L. and A. BELLON. 1974. The use of digital weather radar records for short term precipitation forecasting. *Quart. J. Roy. Meteorol. Soc.* **100**: 658–664.

BARRETT, E. 1970. Estimation of monthly rainfall from satellite data. *Mon. Wea. Rev.* **98**: 322–327.

BELLON, A. and G.L. AUSTIN. 1978. The evalu-

ation of two years of real time operation of a short-term precipitation forecasting procedure (SHARP). *J. Appl. Meteorol.* (in press).

BLACKMER, R. 1975. Correlation of cloud brightness and radiance with precipitation intensity. Stanford Res. Inst. Menlo Park, CA. Final Report – Task B (NEPRF TR8-75 (SRI)).

CHENG, N. and D. RODENHUIS. 1977. An intercomparison of satellite images and radar rainfall rates. Tech. Rep. 77–166, Meteorol. Program, Univ. Maryland, College Park, 60 pp.

FOLLANSBEE, W.A. 1973. Estimation of average daily rainfall from satellite cloud photographs. NOAA Tech. Memo. NESS 44.

——— and V.J. OLIVER. 1975. A comparison of infrared imagery and video pictures in the estimation of daily rainfall from satellite data. NOAA Tech. Memo. NESS 62.

———. 1976. Daily precipitation over China and USSR using satellite imagery. NOAA Tech. Memo. NESS 81.

GRIFFITH, C.G.; W.L. WOODLEY, P.G. GRUBE, D.W. MARTIN, J. STOUT and N.D. SIKDAR. 1978. Rain estimation from geosynchronous satellite imagery. *Mon. Wea. Rev.* **106**: 1153–1171.

INGRAHAM, D.; J. AMOROCHO, M. GUILARTE and M. ESCALOVER. 1977. Preliminary rainfall estimates in Venezuela and Columbia from GOES satellite images. Published in preprint volume on the Second Conference on Hydrometeorology, 25–27 Oct.

KILONSKY, B.J. and C.S. RAMAGE. 1976. Technique for estimating tropical open-ocean rainfall from satellite observation. *J. Appl. Meteorol.* **15**: 972–975.

LOVEJOY, S. 1978. The relationship between coarse resolution satellite data and area of rain. Fourth Symposium on Meteorol. observations and instrumentation. Amer. Meteorol. Soc., Boston, Mass.

SCOFIELD, R.A. and V.J. OLIVER. 1977a. A scheme for estimating convective rainfall from satellite imagery. NOAA/NESS Tech. Memo. 86, 47 pp.

——— and ———. 1977b. Using satellite imagery to estimate rainfall from two types of convective systems. 11th Conference on Hurricanes and Tropical Meteorol. Miami, Dec. 13–16. Amer. Meteorol. Soc., Boston, Mass.

SIKDAR, P.N. 1972. ATS-3 observed cloud brightness field related to a meso-synoptic scale rainfall pattern. *Tellus*, **24**: 400–413.

SILVA DIAS, P.L.; M.F. SILVA DIAS and A.E. SMITH. 1977. A possible relationship between satellite derived temperature and brightness and radar precipitation estimates in GATE. Atmos. Sci. Dept., Colorado State University.

STOUT, J.; D. MARTIN and D.N. SIKDAR. 1977. Rainfall estimation from geostationary satellite images over GATE area. 11th Tech. Conference on Hurricanes and Tropical Meteorology. Amer. Meteorol. Soc., Boston, Mass.

WILHEIT, T.T.; A.T.C. CHANG, M.S.V. RAO, E.B. RODGERS and J.S. THEON. 1977. A satellite technique for quantitatively mapping rainfall rates over the ocean. *J. Appl. Meteorol.* **16**: 551–560.